Iterative Machine Learning-Aided Framework Bridges Between Fatigue and Creep Damages in Solder Interconnections

Vahid Samavatian, Mahmud Fotuhi-Firuzabad, *Fellow, IEEE*, Majid Samavatian, Payman Dehghanian, *Senior Member, IEEE*, and Frede Blaabjerg, *Fellow, IEEE*

***Abstract*— Costly and time-consuming approaches for solder joint lifetime estimation in electronic systems along with the limited availability and incoherency of data challenge the reliability considerations to be among the primary design criteria of electronic devices. In this article, an iterative machine learning framework is designed to predict the useful lifetime of the solder joint using a set of self-healing data that reinforce the machine learning predictive model with thermal loading specifications, material properties, and geometry of the solder joint. The self-healing dataset is iteratively injected through a correlation-driven neural network (CDNN) to fulfill the data diversity. Outcomes show a very significant enhancement in lifetime prediction accuracy of the solder joint within a very short time. The effects of solder alloy and solder layer geometry are separately evaluated on the creep-fatigue damage evolution of the solder joint. The results reveal that Sn–Ag–Cu-based solder alloy generally has a better performance. Moreover, the creep and fatigue damage evolutions are found dominant, respectively, in Sn–Pb- and Sn–Ag–Cu-based solder alloys. The proposed framework offers a tool allowing for the reliability-driven design of electronic devices in the early stage of fabrication.**

***Index Terms*— Creep damage, electronic device, fatigue damage, iterative machine learning, solder joint.**

I. Introduction

In THE last few years, there has been a growing interest in strengthening electronic devices under harsh environmental conditions in a variety of applications, such as satellites in space, aircraft, and vehicles [1]–[3]. Power semiconductors are known among the most vulnerable parts in electronic circuits [4]. Within the power semiconductors, solder joints' strength in facing external and internal stresses has remained a long-lasting challenge for manufacturers [5]–[7]. The solder joints encounter considerable thermomechanical stresses during their normal working conditions, which, consequently, shortens the useful lifetime of the devices [8].

Numerous studies have focused on the existing challenges around reliability evaluation of the solder joints in order to discover the effects of different contributory factors on the lifetime of the power devices. For several years, great effort has been devoted to the study of factors, such as mechanical properties, current stress, thermal variations, intermetallic formation, phase transition, and defects nucleation to estimate the useful lifetime of the solder joints in electronic devices. For instance, Siswanto *et al.* [9] discussed the effect of the electric current on the microstructure and degradation performance of the solder joints, resulting in an optimum layer thickness for the solder joint. The effects of current waveforms on the useful lifetime of the solder joint were investigated in [10], revealing that square wave has comparably the lowest failure resistance. Although these studies assessed the significance of the current in the solder joint lifetime, they were not able to include other important contributory factors. A considerable number of studies on the constitutive models with the diverse range of strain rate and the temperature were performed to tackle the inconsistencies in the conventional models and suggested predictive frameworks founded based on correlations among the physical parameters [10], [11]. Thermal-related specifications have been reflected in numerous studies [12]–[17]. Multifactor impacts of the junction temperature swing in power modules were considered in the power cycling tests and, consequently, useful lifetime estimation of the solder joint employing several failure indicators, including thermal and electrical resistances and ON-state voltage of the devices [18]. The effect of thermal-related specifications on SiC power devices at high temperature (200 °C) was studied in [19], where an ultrafast and miniaturized system was proposed with an added online thermal characteristic measurement function to characterize the effect of high temperature on the reliability of the solder joint. A layer thickness optimization was carried out under fixed thermal and mechanical conditions in [20]. This optimization was based on the creep energy accumulation in the solder joint and its thermal resistance in the power devices.

Manuscript received April 16, 2021; revised November 3, 2021; accepted December 14, 2021. Date of publication December 20, 2021; date of current version February 23, 2022. This work was supported in part by the Reliable Power Electronics-Based Power System (REPEPS) Project at the Department of Energy Technology, Aalborg University, as a part of the Villum Investigator Program funded by the Villum Foundation. Recommended for publication by Associate Editor C. J. Bailey upon evaluation of reviewers' comments. *(Corresponding author: Mahmud Fotuhi-Firuzabad.)*

Vahid Samavatian and Mahmud Fotuhi-Firuzabad are with the School of Electrical Engineering, Sharif University of Technology, Tehran 68260, Iran (e-mail: vahid.samavatian@sharif.edu; fotuhi@sharif.edu).

Majid Samavatian is with the Department of Advanced Materials and Renewable Energy, Iranian Research Organization for Science and Technology (IROST), Tehran 3313193685, Iran (e-mail: m.samavatian@srbiau.ac.ir).

Payman Dehghanian is with the Department of Electrical and Computer Engineering, George Washington University, Washington, DC 20052 USA (e-mail: payman@gwu.edu).

Frede Blaabjerg is with the Department of Electrical Engineering, Aalborg University, 9100 Aalborg, Denmark (e-mail: fbl@et.aau.dk).

Color versions of one or more figures in this article are available at https://doi.org/10.1109/TCPMT.2021.3136751.

Digital Object Identifier 10.1109/TCPMT.2021.3136751

Lee *et al.* [21] proposed a new acceleration factor for the reliability assessment of the solder joint based on different thermal cyclic loading rates. The theory was reconfigured in [22] by enfolding the mechanical loading with the thermal-related specifications to estimate the fatigue lifetime of the electronic devices. All the above studies were using a unilateral analysis of a limited number of contributory factors due to physical limitations. Thereby, a decisive difference between the models and experimental results has motivated researchers and developers to envision realistic models capable of capturing all contributory factors. Statistical methods, such as Weibull distribution [23], offer promising potential in this regard. The uncertainties in physical parameters were taken into account using the Weibull distribution for lifetime modeling of the solder joint in the power devices [24], [25]. With Weibull-distributed data and several nonlinear models employed, solder chemical composition, thermal-related specifications [26], and solder joint geometry [27] are found as the key parameters in stimulating the failure mechanism of the solder joint. Ma *et al.* [28] declared that the failure rate in the solder joints depends heavily on the size of the package and the metallurgical aspect of the solder material. Hazard regression analysis was proposed by Raj *et al.* [5] to appropriately estimate the useful lifetime of the solder joint, where the aging conditions of the solder joint and its composition were found as the primary factors in the solder joint degradation. More previous research [29]–[31] had focused on the reliability assessment of the power converters based on a range of fundamental principles in handbooks, such as MIL-HDBK-217 [32] and IEEE 1413.1 [33]. These studies focused on the reliability of the system with no consideration to the physical aspects of the failure. Lack of intuition on either failure mechanisms or failure root causes soon led to such stochastic models not being widely utilized in practice. On the other side, more recently, machine learning methodologies are used for the reliability assessment of electronic devices [34]–[36]. Machine learning is able to bridge a meaningful correlation among the substantial contributory factors and strength of the solder joint under different conditions. However, ample and adequate datasets are required in the training phase of the machine learning algorithms in order to establish an acceptable predictive model for lifetime estimation of the solder joint in electronic devices. Collecting the training datasets either from simulations or experiments is critical in developing a precise predictive model. Although several studies [37]–[40] have dealt with different types of artificial networks in technical designs, little attention has been given to the use of machine learning for lifetime prediction of the solder joints in electronic devices. Sung and Robert [41] declared that artificial network-based reliability assessment of the solder joint may engender a much more accurate outcome provided that the training datasets are both accurate and adequate alike.

Samavatian *et al.* [36] draw attention to a new research direction suggesting to use a correlation-driven neural network (CDNN) proposed for evaluating the useful lifetime of the solder joint in power devices. Multiple contributory factors of composition (material and physical properties of the joint zone), thermal loading specifications and solder joint geometry were judiciously considered in the lifetime estimation. However, it does not investigate the effects of solder joint geometry on the fatigue evolution within the devices. Similarly, the most critical factors, such as high and low dwelling temperatures, dwelling times, and ramping rates, were ignored in [36]. Enriching data on the above critical conditions calls for several costly and time-consuming experiments and simulations particularly in low dwelling temperatures, dwelling times, and ramping rates. For instance, implementing an experiment in low-intensity thermal conditions was taking at least six months [42]. Even though reliability assessment of the solder joints has been improved using the suggested CDNN platform in [37], such improvements have been found to be limited by inadequate training datasets, especially in low-/high-intensity thermal conditions. Nonetheless, it is possible to further improve the accuracy of the predictive model by creating data through a self-training algorithm. With the goal to fill in the mentioned knowledge gap in the state-of-the-art literature, this work seeks to fortify the training datasets for the more promising performance of the CDNN predictive model, which was previously proposed by Labed and Labed [37]. We develop and validate the CDNN approach for reliability assessment of the solder joints and bridge solder joint geometry with the fatigue damage evolution in electronic systems in order to optimize the best geometry conditions. The developed CDNN model results in an accelerated discovery of the effects of the important contributory factors on the useful lifetime of the solder joint.

The remainder of this article is structured as follows. Section II introduces the proposed methodology. Numerical evaluation of the proposed framework and the results are discussed in Section III. Finally, conclusions are drawn in Section IV.

II. Methodology

Artificial intelligence is a tool to estimate a specific variable through learning some historical examples or past experiences. Two main steps are considered in the conventional cognitive process of a machine learning algorithm. The data collection process sets forth the attributes influencing the output (i.e., the useful lifetime of the solder joint in electronic devices). For a specific type of fabrication and packaging technology (here, the considered power semiconductor packaging is TO220), the contributory attributes for accurate estimation of the solder joint's useful lifetime can be classified into three main categories, including thermal loading specifications, chemical compositions (mechanical and physical properties), and solder joint geometry [36]. The next step is to train a predictive model for the considered output using the contributory attributes. There exist several machine learning principles that could be employed to train the predictive model, including the conventional methods, correlation-driven approaches, and so on. CDNN, proposed by Samavatian *et al.* [36], is employed in this study founding the training algorithm. Fig. 1 demonstrates the pictorial description of the CDNN structure (blue sections). A set of relevant data as the main contributory factors affecting the targeted output was either collected or

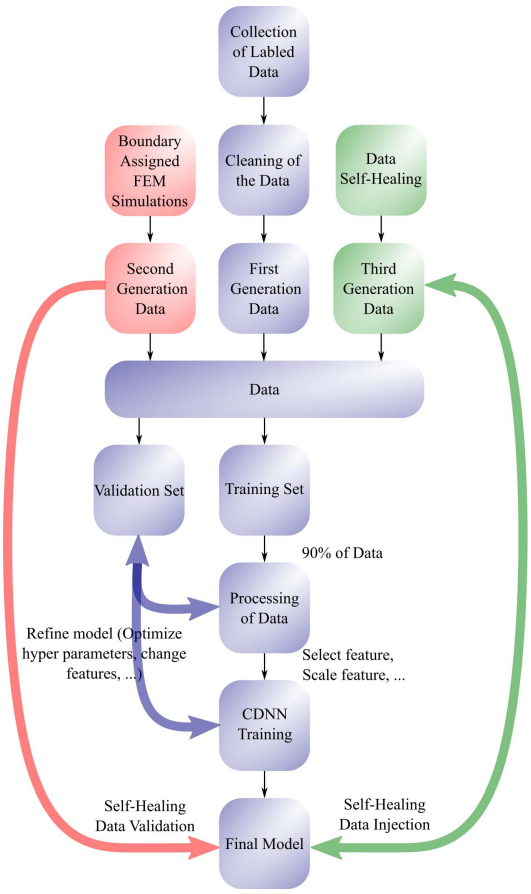

Fig. 1. Workflow of the proposed iterative machine learning-aided framework for assessing the lifetime of the solder interconnections.

created if necessary. The collected and created data need to be cleaned in order to guarantee their accuracy for training the predictive model. Some data need to be translated from raw information (contributory factors) into given features (attributes), which are the main inputs of the CDNN. With the attributes processed, the predictive model will be trained using the CDNN algorithm. Some of the data are considered for validation and optimization of the predictive model.

A. Database

Collecting and creating adequate input data are of paramount importance in the training process of a predictive model. In this study, we use our previous publicly available resources [3], [36], [42] and strengthen our input data by performing some boundary-embedded finite element method (FEM)-based simulations and some self-healing data (the strengthening data will be discussed in Sections II-C–II-E). Details on the FEM procedure, conducted by Surendar *et al.*, are provided in [43] and are available in the Appendix. The data are cleaned and made ready for the new training process. The data include the thermal loading specifications, joint compositions (physical and material properties of the joint zone), and solder joint geometry. Together with these feature attributes, the useful lifetime of the solder joints in electronic devices as the target outputs is collected [3], [36], [42]; 390 simulation and 60 experimental datasets are directly

TABLE I

USED PHYSICAL PROPERTIES, THERMAL LOAD SPECIFICATIONS, AND GEOMETRY FEATURES OF THE SOLDER INTERCONNECTIONS

Thermal load specifications	Joint Zone specifications	Geometry
Dwelling temp. (°C)	SJ/U/B Melting Temp. (°C)	Thickness (um)
	SJ/U/B Poisson ratio	Length (mm)
Dwelling time (min)	SJ/U/B Young Module (GPa)	Width (mm)
	SJ/U/B CTE (10^{-6}/ °C)	
Ramping rate (°C /min)	SJ/U/B Density (g/cm^3)	

SJ: Solder Joint U/B: Upper/Basal Temp: Temperature
CTE: coefficient of thermal expansion

extracted from the authors' previous works concentrating on the TO220-package power devices under diverse loading and physical conditions. The consistency between the FEM and experimental results was discussed in [36]. In addition to the above 450 datasets, 300 datasets are provided with the new FEM simulations and self-healing iterative algorithms considering different loading and physical conditions.

B. Featured Attributes

Featured attributes ($\mathbf{X}$) are considered as the inputs to the CDNN model (f) for predicting the target output (Y), i.e., $Y = f(\mathbf{X})$. The more precise and sufficient $\mathbf{X}$ is, the more accurate prediction of the target output Y will be achieved. Not only do sufficient featured attributes affect the accuracy of the output but also it can accelerate the discovery of the damage evolution occurring in the solder joint material. The featured attributes are listed in Table I. These parameters highly influence the performance of the solder joint in electronic devices. In order to improve the training process, these featured attributes are normalized into a specific range, namely, [0.2 0.8], as follows:

$$x_{\text{new}} = 0.2 + \frac{(0.8 - 0.2)(x - \min(x))}{\max(x) - \min(x)} \tag{1}$$

where x and x_{new} are the original and the scaled featured attributes, respectively. 0.2 and 0.8 are selected as the lower and upper boundaries, which were proven acceptable and efficient in the previous reports [36], [44], [45].

C. CDNN Model

There exist several algorithms for training a predictive model seeking a target output, ranging from linear algorithms, nonlinear algorithms, and ensemble algorithms that have been employed in the previous literature [44], [46]. In this study, the CDNN framework, introduced by Samavatian *et al.* [36], is used and further developed. CDNN is capable of considering the correlations among the feature candidates, leading to much more precise predictions. The algorithm contains two unique paths and follows by a deep neural network, usually known as fully connected layers (FCLs). A path belongs to the correlated data in which the input feature candidates correlate each other via the trained correlation matrices (the elements would be derived during the training process). CDNN may have a stack of multiple correlating, activating, and pooling layers. Predictably, the more layers are employed, the less error will

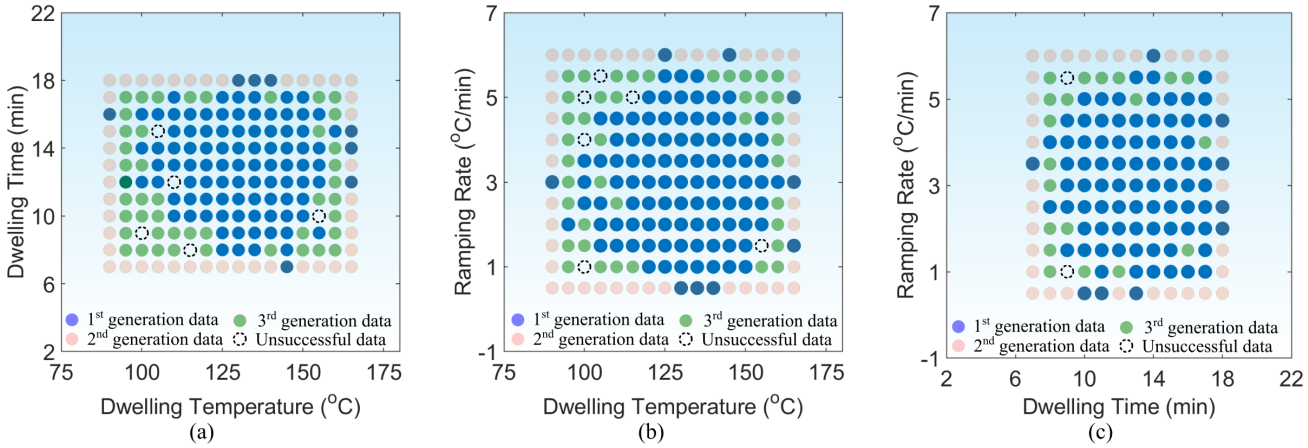

Fig. 2. Spread out of three major thermal loading specifications, including (a) dwelling temperature-dwelling time, (b) dwelling temperature-ramping rate, and (c) dwelling time-ramping rate considered as the featured attributes.

exist at the expense of longer computation time. In this study, rectified linear unit (ReLU) functions and average pooling were used as the activation function and the pooling method, respectively. The second path directly transfers the feature candidates to the deep neural network. Thus, both individual and mutual effects of the feature candidates have been properly considered in this novel approach, which is expectedly leading to more accurate results. Capturing the correlations among the feature candidates makes the CDNN more precise and faster compared to the conventional neural network (CNN) practices. The detailed information on the CDNN predictive model is available in [36].

D. Iterative CDNN

Although the proposed CDNN mode is capable of capturing the correlations among the inputs leading to much higher accuracy, it lacks the ability to capture low-/high-intensity thermal loading conditions regarding the sparse input data. The occurrence of low-/high-intensity thermal loading conditions is reported in several applications [47]–[49]. Since creating data either from simulations or experiments is too time-consuming and costly, we further develop the proposed CDNN algorithm by integrating several additional paths into the framework shown with green and red sections in Fig. 1. In this procedure, two new-generation datasets are added to the input data in order to complete the data range for better performance of the predictive model. The first-generation dataset is unchanged with regard to the previously proposed CDNN in [37]. 90% of the first-generation data were included in the training process, and the remaining 10% were used for the accuracy verification of the proposed ICDNN prediction model. Fig. 2 demonstrates the dispersion of three major thermal loading specifications, including dwelling temperature, dwelling time, and ramping rate, all of which are considered as the featured attributes in the model training (see Table I). The first generation data are shown with blue filled circles. As it can be seen from Fig. 2, the dispersion of data is sparse, and several important conditions are missing. These conditions may occur in a variety of applications, and consequently, an acceptable lifetime prediction of the solder joint calls for a sufficient number of featured attributes. In order to fulfill the data requirements, boundary-imposed FEM simulation datasets are defined as shown with filled red circles in Fig. 2. The boundary-embedded FEM simulation data aim to determine and complete the boundary conditions, the lack of which may occur in real applications. We call these data the *second-generation data,* which is directly involved in the training process of the CDNN. Second-generation data are also used for validating the self-healing data to fulfill the database requirements. Including filled red and blue data shown in Fig. 2, there exist a lot of missing data points in the data region. Therefore, it is required to perform some simulations or experiments to investigate the damage evolution of the solder joint in electronic devices. Since the number of missing data is considerable and the experiments are time-consuming, we propose an iterative CDNN (ICDNN) for training the predictive model. The predictive model is iteratively updated and healed with the arrival of new self-healing data. In this regard, a set of self-healed data, shown with filled green circles in Fig. 2, is applied to the trained predictive model to fulfill the data dispersion. The predicted output of each self-healing data is compared to the vicinity actual data (measured and simulated) and is considered in the training process, provided that it satisfies a predefined range of error. If the error limits are violated, the specified self-healing data are eliminated from the training process, called *unsuccessful self-healing data,* which are shown by dashed circles in Fig. 2. Therefore, the ICDNN algorithm can be implemented through the following steps.

1) The database is processed and cleaned. The most critical featured attributes (i.e., thermal loading specifications) are chosen, and their dispersions across each other are determined. Based on this analysis, some boundary conditions are characterized with which the FEM simulations or experiments are performed in order to increase the database density.
2) Both initial data (blue circles) called *first-generation data* and those from the boundary-embedded FEM simulation (red circles) called *second-generation data* are used in the training process of the predictive model.

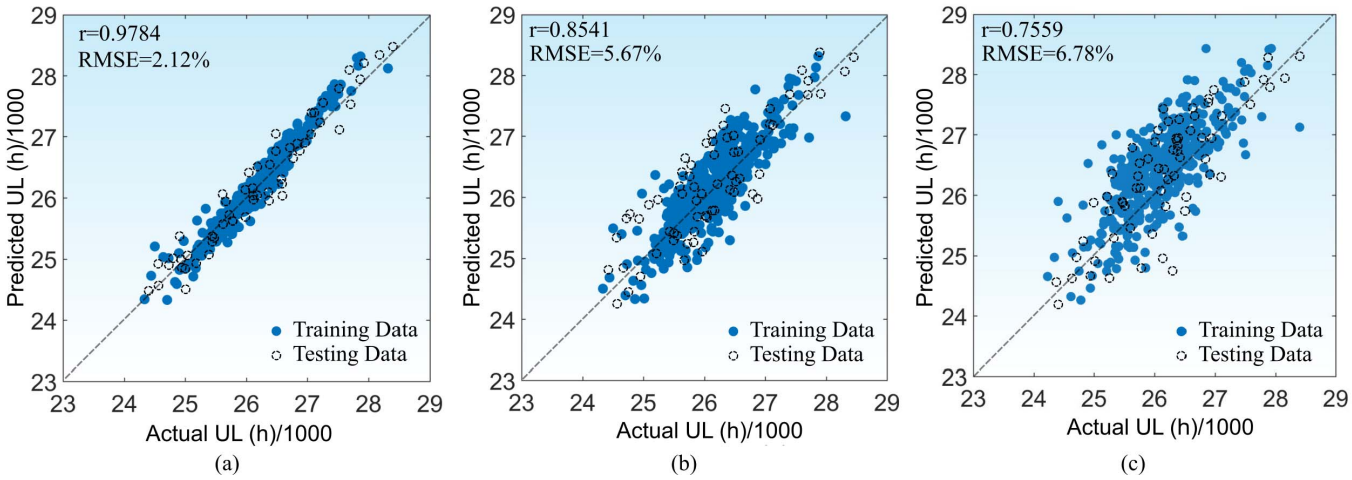

Fig. 3. Neural network predicted values versus the actual values. (a) Iterative CDNN, (b) CDNN, and (c) CNN.

3) Then, self-healing data, needed to fulfill the data dispersion (green circles) called *third-generation data*, are applied to the trained predictive model. The predicted target output (i.e., the useful lifetime of the solder joint) is compared with the actual useful lifetime of the solder joint in the vicinity of the input data, including the first- and second-generation datasets. The self-healing data are involved in the next training process provided that its predicted output is sufficiently close to the vicinity-actual output with the prespecified error (here, assumed to be $+/-5\%$).
4) This training process is iteratively performed until all the self-healing data are considered. During this step, the self-healing data, which violates the predefined error, maybe crossed out from the training process. All other featured attributes, including the joint chemical composition and its geometry, are considered randomly within the maximum and minimum of the first-generation database.

E. ICDNN Performance

The performance and ability of the proposed model may be quantified by comparing the actual and predicted target outputs. The performance of the regression models is calculated using the correlation factor r [44]

$$r = \sqrt{\sum_{i=1}^{n} (\hat{y}_i - \bar{y})^2 \Big/ \sum_{i=1}^{n} (y_i - \bar{y})^2} \tag{2}$$

and the root mean square error (RMSE)

$$\text{RMSE} = \sqrt{\sum_{i=1}^{n} \frac{1}{n} (\hat{y}_i - y_i)^2} \tag{3}$$

where $\hat{y}_i$, y_i, and $\bar{y}$ are predicted, actual, and mean values of the actual output, respectively. r values are within [0 1], where 1 represents the perfect fit.

III. Numerical Results and Discussions

A predictive model was trained using the proposed ICDNN algorithm in order to estimate the useful lifetime of the solder joint in electronic devices. To demonstrate the performance of the proposed iterative algorithm, the predicted results of the target output (i.e., the useful lifetime of the solder joint) are compared to the actual target output using three different training processes, namely, CDNN, ICDNN, and CNN. The results are shown in Fig. 3. 80 correlation matrices were considered with the dimensions of 3×3, where three hidden layers exist in the algorithm with the same number of neurons (50) for all frameworks [36]. Using the same computing system, the elapsed times were estimated 618, 103, and 76 s for ICDNN, CDNN, and CNN, respectively. Although the training time was increased six times, one can see that the proposed ICDNN framework offers a more trustworthy performance in lifetime estimation of the solder joint in electronic devices. As mentioned, 10% of the data were not included in the training process in order to investigate the performance of the prediction model. Regarding Fig. 3, the testing data can verify that the accuracy of the lifetime prediction model is adequately acceptable in all frameworks (the ICDNN algorithm has the best performance). As mentioned earlier, two different sets of data, i.e., the boundary-embedded and self-healing datasets, were included in the training process in order to enhance the performance and validity of the predictive model. The RMSE values of the CNN, CDNN, and ICDNN models are limited to 6.78%, 5.67%, and 2.12%, respectively. It reveals that the rms error between the predicted and the actual target output is by far lower in ICDNN than that of the CDNN and CNN, further highlighting the more acceptable performance of the proposed ICDNN algorithm. This observation is further supported by the much higher correlation factor in the ICDNN compared to the CNN and CDNN algorithms. The correlation factors calculated ate 0.9784, 0.8541, and 0.7559 for ICDNN, CDNN, and CNN, respectively. This indicates that the new model includes two new sets of data in the training process offering a more accurate prediction. The reason, of course, is originated from the fact that the database was thoroughly

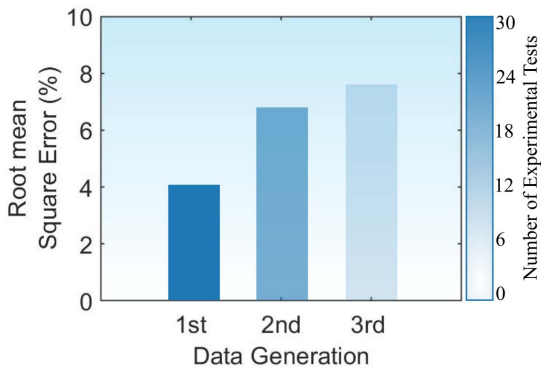

Fig. 4. Comparison between the experimental solder joint lifetime measurements and the FEM and the self-healing solder joint lifetime estimation.

healed and fulfilled via injecting new datasets and conducting the training process iteratively. In this case, missing input data could be reconstructed in the training process, leading to higher accuracy of the predictive model. For evaluating the accuracy of the input datasets, including the first, second, and third datasets, the predicted solder joint useful lifetime is compared to the actual lifetime under the same loading and physical conditions. In this regard, Fig. 4 demonstrates the RMSE between the actual and the predicted solder joint lifetime for the individual datasets. As can be seen, there exists 4.1% error between the FEM-based simulation and the experimental results for the first generation data. The RMSEs are 6.8% and 7.9% for the second- and third-generation data, respectively. Generally, the estimated solder joint lifetime is in good agreement with the experimental results. The individual results were also studied, where it is found that the largest error was directed to the Sn–Pb solder joint in which insufficient data were collected or created. Overestimation in the predictive model was trigged whenever the base materials are aluminum, as was also reported in [36]. In contrast with the results reported in [36], no considerable underestimations were reported due to the proposed iterative framework. A few data points appear still farther than the ideal dashed line, which may be due to the inaccuracies in experimental tests or simulation outcomes of the literature.

The dwelling time, temperature, and ramping rate are the main failure activations that can directly stimulate the creep and fatigue failure mechanisms inside the solder joint in electronic devices. Conventionally, creep and fatigue are considered as two separate failure mechanisms for which the associated damage may linearly accumulate and expedite the global failure in the electronic devices [50–[53]. However, the coupling effects among these two failure mechanisms have significant physical impacts on the degradation of the solder joint. It was proven that the creep phenomena may alter the mechanical properties of the solder joint, which finally affects its failure mechanism [54]. The results reported in [55] have validated the increase in the shear strength as the creep strain rate increases. According to (4), the solder joint ductility decreases as the creep strain rate increases [42], [56], [57]

$$\varepsilon'_f = \varepsilon'_{f0} - p\ \log \dot{\varepsilon}_c \tag{4}$$

where p is the material-dependent coefficient extracted from the ductility and the strain rate fitting under the material experiments, ε'_{f0} is the initial fatigue ductility coefficient, and $\dot{\varepsilon}_c$ is the stable creep strain rate. Hence, the well-known Coffi–Manson fatigue lifetime model may be written as follows [58]:

$$\frac{\Delta\varepsilon_p}{2} = \left(\varepsilon'_{f0} - p\ \log \dot{\varepsilon}_c\right)(2N_F)^c \tag{5}$$

where $\Delta\varepsilon_p$ is the plastic strain induced in the solder joint, while N_F and c are the number of cycles to the failure and material-dependent fatigue ductility exponent, respectively. Using linear damage accumulation, one can express the one-cycle damage as follows:

$$D_F = \frac{1}{N_F} = 2\left(\frac{\Delta\varepsilon_p}{2\left(\varepsilon'_{f0} - p\ \log \dot{\varepsilon}_c\right)}\right)^{-\frac{1}{c}}. \tag{6}$$

For n-cyclic loads during a period of time, the accumulated damage can be written as follows:

$$D_F(t) = \sum_{i=1}^{n} \frac{1}{N_{\mathrm{Fi}}} = \sum_{i=1}^{n} 2\left(\frac{\Delta\varepsilon_{pi}}{2\left(\varepsilon'_{f0} - p\ \log \dot{\varepsilon}_c\right)}\right)^{-\frac{1}{c}}. \tag{7}$$

Consequently, the aforementioned damage can be considered as two separate damages, as shown below

$$D_F(t) = D_f(t) + D_{\mathrm{fc}}(t) \tag{8}$$

where D_f is the pure fatigue damage and D_{fc} is the damage originated from the coupling effects of the creep on the solder joint fatigue lifetime.

On the other side, the applied stress σ_D at the accumulated damage D can be determined as

$$\sigma_D = \frac{\sigma_0}{1 - D} \tag{9}$$

where σ_0 is the initial applied stress and D is the global accumulated damage originated from both fatigue and creep phenomena. Regarding (9) and the working environment of the solder joint, including severe cyclic loads and ongoing high temperature, the creep strain rate can be written as follows [42]:

$$\dot{\varepsilon}_c(D(t)) = A\left(\frac{\sigma_0}{1 - D}\right)^n \exp\left(\frac{-Q}{RT}\right) \tag{10}$$

where A and n are the material-dependent coefficient and exponent, respectively. R, Q, and T are universal gas constant, activation energy, and absolute temperature, respectively.

Accordingly, the evolved creep damage can be formulated as follows using the Monkma–Grant model [42]

$$D_C(t) = \frac{\Delta t}{t_c} = \Delta t\left(\frac{\dot{\varepsilon}_c(D(t))}{C_{\mathrm{MG}}}\right)^{\frac{1}{\beta}} \tag{11}$$

where C_{MG} and β are material-dependent constant and exponent, respectively. Δt is the dwelling time at which the solder joint is subjected to high absolute temperature.

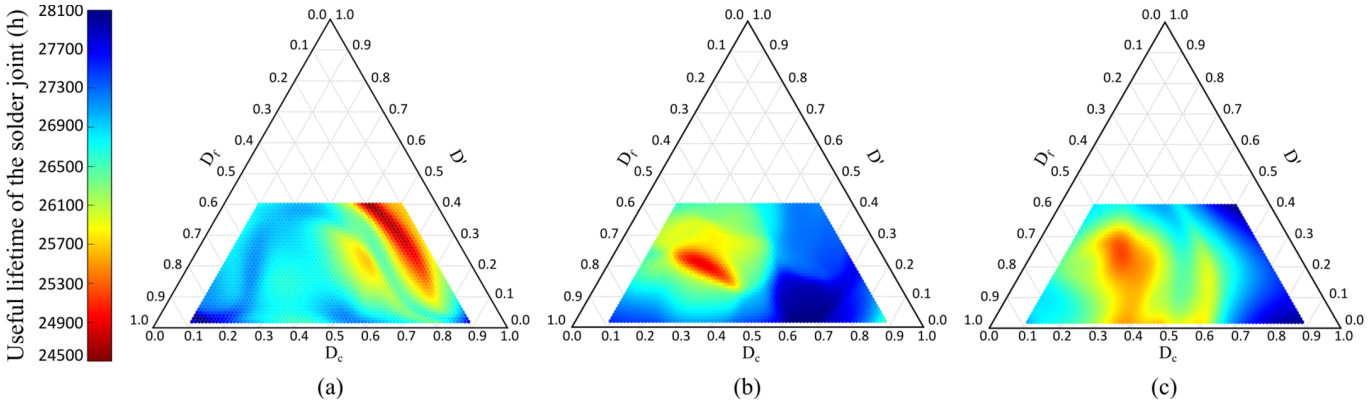

Fig. 5. Ternary useful lifetime distribution map of the solder joint considering different damage partitions for (a) Sn–Pb, (b) SAC305, and (c) SAC387 solder alloys.

Consequently, the aforementioned damage can be considered as two separate damages, as given below

$$D_C(t) = D_c(t) + D_{\mathrm{cf}}(t) \tag{12}$$

where D_c is the pure creep damage and D_{cf} is the damage originated from the coupling effects of the fatigue on the solder joint fatigue lifetime. In this regard, one can assume that there exist three damage evolutions in the global solder joint aging mechanism as follows:

$$D(t) = D_c(t) + D_f(t) + D'(t) \tag{13}$$

where

$$D'(t) = D_{\mathrm{fc}}(t) + D_{\mathrm{cf}}(t). \tag{14}$$

Hence, a ternary analysis is required as defined in (13) in order to capture the coupling effects of the creep and fatigue phenomena on the damage evolution of the solder joint. Mathematically, one can consider the failure occurrence in the solder joint provided that the sum of the ternary damages reaches one. For further explanation, a ternary map of the useful lifetime is taken into account in order to investigate the effects of different damages on the solder join's lifetime. In this regard, three different widely-used solder alloys, namely, SnPb, SAC305, and SAC387, were studied, each of which comprises different mechanical properties that affect the solder joint aging. Extracted from the ICDNN machine learning algorithm, the ternary useful lifetime map is illustrated in Fig. 5. The ternary maps were constituted with the vicinity of different damages, as shown in (13). Each of the ternary points in the map was achieved by adjusting the thermal cycling load specifications, including the dwelling time, the dwelling temperature, and the ramping rate [20], [36]. It was proven that the ramping rate has the most influence on the fatigue damage evolution, while the dwelling temperature and time have the most effects on the creep damage evolution [42]. Meanwhile, due to the coupling effects between the fatigue and creep phenomena, the thermal cycling load specifications may affect both creep and fatigue damage evolutions. For this reason, trial and error were employed in order to provide a unique ternary point in the solder joint lifetime map. The geometry of the solder joints was kept identical for all solder alloys. From this figure, one can find that the performance of the SAC387 under different temperature cycling loads was generally better in comparison with other solder alloys. The minimum useful lifetimes of the solder joints are found 24 485, 25 232, and 25 717 h for SnPb, SAC305, and SAC387, respectively. The asymmetrical useful lifetime map is due to the diverse mechanical properties of the solder joints from SnPb to SAC solder alloys. For SnPb solder alloy [see Fig. 5(a)], it is observed that the lowest useful lifetime of the solder joint was realized in the higher creep damage zone ($0.35 < D_c < 0.75$) and the lower fatigue damage zone ($0.10 < D_f < 0.22$). In this condition, the remaining damage evolution belonged to fatigue-creep coupling damage. For the SAC305 solder alloy [see Fig. 5(b)], the most vulnerable zone was found in the higher fatigue damage ($0.45 < D_f < 0.70$) and lower creep damage ($0.10 < D_c < 0.30$) regions. In this condition, the remaining damage evolution belonged to the fatigue-creep coupling damage. For the SAC387 solder alloy [see Fig. 5(c)], the map shows a more outspread condition in which the lowest useful lifetime of the solder joint occurred in creep damage zone of $0.20 < D_c < 0.55$ and the fatigue damage zone of $0.30 < D_f < 0.75$. It was also revealed that the creep damage has a lower share in the global aging of the solder joint in SAC-based solder alloys, while the Pb-based solder alloy suffers more from fatigue damages. These observations are primarily driven by the material and mechanical properties of these solder alloys. SAC-based solder alloys with a higher young module (50 and 61.2 GPa for SAC305 and SAC387, respectively) and higher melting temperatures (220 °C and 217 °C for SAC305 and SAC387, respectively) in comparison with Pb-based solder alloys with a young module of 32 GPa and melting temperature of 183 °C show more obstruction against creep mechanism. However, the creep phenomenon is more critical to SnPb solder alloy due to its lower melting temperature. These mechanical properties also lead to higher fatigue damage in SAC-based alloys in comparison with SnPb-based solder alloys.

From a geometry point of view, we focus on as the most important geometry parameter in the solder joint aging and consider different solder joint thicknesses from 30 to 50 μm to analyze the effect of solder layer thickness on the damage

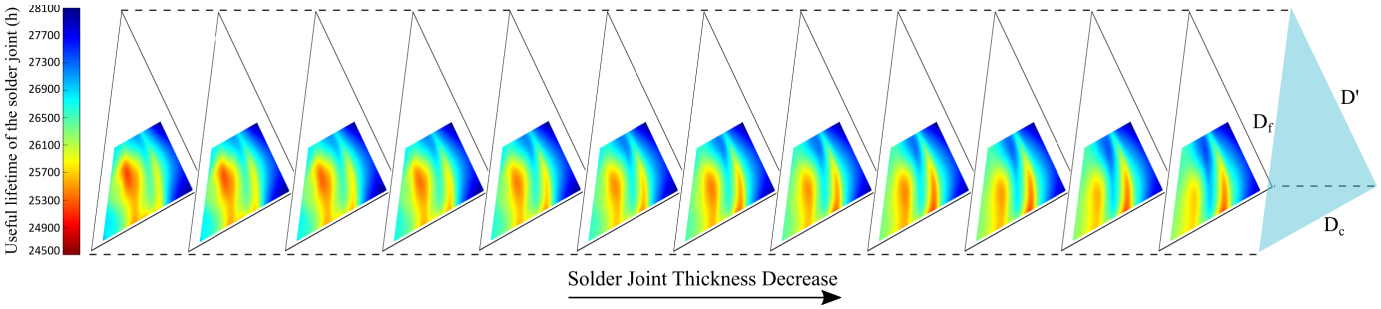

Fig. 6. Quaternary solder joint lifetime distribution map as the solder layer thickness decreases.

distribution and lifetime ternary map [20], [42]. In this regard, we considered the SAC387 solder alloy with the above same conditions but with different solder joint thicknesses. The ternary useful lifetime maps were extracted from our proposed ICDNN machine learning algorithm and constituted a quaternary map including three damages and solder joint thickness, as shown in Fig. 6. One can easily see, from the results in Fig. 6, that, as the thickness decreases, the useful lifetime of the solder joint appears longer, and as the thickness continues declining, it again becomes shorter. Hence, there exists an optimum solder layer thickness with respect to the solder joint useful lifetime. This is primarily due to the failure mechanism trigging in the solder joint and shows that the minimum failure event (damage evolution) may occur in an optimum solder layer thickness. This can be a good starting point when designing the device.

Further evaluating the results shown in Fig. 6, one can find that, as the thickness decreases, the solder joint lifetime map distribution changes correspondingly. At the thicker solder layer, fatigue damage is dominant, and the lowest solder joint lifetime occurs in the vicinity of the maximum fatigue damage. As the solder layer thickness decreases (reaching 40 μm), both fatigue and creep failure mechanisms were equally involved in the solder joint aging. As the solder joint thickness continues to decrease, the creep damage becomes more dominant, and the lowest solder joint lifetime occurs in the vicinity of the maximum creep damage. Accordingly, the thicker the solder layer is, the weaker it will be against the fatigue failure mechanism; similarly, the thinner the solder layer is, the weaker it will be against the creep failure mechanism. Such variations in the lifetime distribution map are justified since, as the thickness decreases, the variation of the energy density in the solder joint became sharper resulting in higher void nucleation in the solder joint [59]. Accordingly, the maximum stored energy would occur in the minimum thickness and activate the creep failure mechanism. At the thicker solder layer, the stored energy density decreases due to the higher solder joint volume, and thus, the creep failure mechanism is weakened in comparison with the thinner solder layer. However, the thicker the solder joint is, the more significant the CTE mismatch role plays in activating and intensifying the fatigue failure mechanism. Hence, the electronic device tolerates more fatigue damage in the maximum thickness. From the solder joint's thickness point of view, a balance between CTE mismatch and the energy density effects occurs in an optimum solder layer thickness.

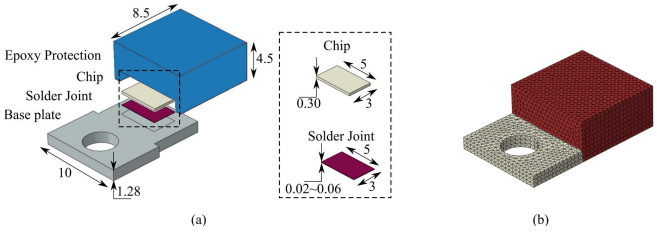

Fig. 7. Discrete To220-package power device. (a) Structure (dimensions in mm). (b) Meshed mode.

IV. Conclusion

This article has established a novel iterative machine-learning-aided framework based on the CDNN to enhance the prediction of the solder joint's useful lifetime. This improvement in the prediction accuracy is achieved by injecting a self-healing dataset to fulfill the data dispersion. In addition to the initial dataset, a boundary-embedded FEM simulation approach was pursued to create and inject a new dataset into the predictive model with the goal of further enhancing the lifetime estimation performance. The results showed a lower RMSE (3.55% reduction) compared to a conventional prediction model. The share of the creep damage, fatigue damage, and creep-fatigue coupling damage was highlighted, while three different solder alloys, including SnPb, SAC305, and SAC387, were employed in the case studies. Ternary damage evolution of the SAC387 joint with a diverse range of solder layer thicknesses was also discussed. It was revealed that, while creep damage is dominant in the thinner solder layer, fatigue damage is the one governing in the thicker solder layer. In this case study, an optimized solder joint was found in which both creep and fatigue damages were at their minimum values.

Appendix
Finite Element Simulation

FEM simulations were employed to characterize the creep and the fatigue behavior of the solder joint under different conditions, namely, thermal loading, chemical composition, and geometry. Hereof, ABAQUS finite element environment was used to investigate the induced thermomechanical stresses and strains in the solder joint. Fig. 7 depicts the TO220-package power semiconductor FEM model with its internal parts. The power semiconductor consists of different parts, including the epoxy, the baseplate, the chip, and the solder

TABLE II
PROPERTIES OF THE DIFFERENT PARTS IN THE POWER SEMICONDUCTORS

Sections	E (GPa)	CTE (10−6/°C)	Poisson's Ratio	Density (×10−6kg/mm3)
SAC305	50.00	21.6	0.36	7.380
SAC387	60.37	20.0	0.36	7.380
63Sn37Pb	32.00	24.7	0.38	8.400
Si Chip	130.0	3.50	0.22	2.330
Cu baseplate	129.0	17.0	0.34	8.690
epoxy	3.000	75.0	0.42	0.300

joint with different material properties, as listed in Table II. Different material and physical properties of the different parts in power devices are known as the primary root cause of failure since they have distinct behaviors under a specific thermal loading condition. The mesh of assembly included 52 300 elements and 73 126 nodes. The joint zone as the most vulnerable part in the semiconductor consists of the solder part, chip, and baseplate. Regarding their physical properties, these materials experienced severe expansion and contraction, which would initiate and propagate voids and cracks in the solder joint. The induced strain in the solder joint characterized by (4) and (10) can be directly extracted from the FEM simulations, which were subsequently employed in the solder joint damage model in (13).

REFERENCES

[1] Y.-W. Chang *et al.*, "Electromigration mechanism of failure in flip-chip solder joints based on discrete void formation," *Sci. Rep.*, vol. 7, no. 1, Dec. 2017, Art. no. 17950.

[2] R. Sayyadi and H. Naffakh-Moosavy, "The role of intermetallic compounds in controlling the microstructural, physical and mechanical properties of Cu-[Sn-Ag-Cu-Bi]-Cu solder joints," *Sci. Rep.*, vol. 9, no. 1, Dec. 2019, Art. no. 8389.

[3] V. Samavatian, "A systematic approach to reliability assessment of DC-DC power electronic converters," Univ. Tehran Grenoble Alpes, Grenoble, France, Tech. Rep. tel-02302571, 2019.

[4] M. Andresen, K. Ma, G. Buticchi, J. Falck, F. Blaabjerg, and M. Liserre, "Junction temperature control for more reliable power electronics," *IEEE Trans. Power Electron.*, vol. 33, no. 1, pp. 765–776, Jan. 2018.

[5] A. Raj *et al.*, "Thermal shock reliability of isothermally aged doped lead-free solder with semiparametric estimation," *IEEE Trans. Compon., Packag., Manuf. Technol.*, vol. 9, no. 6, pp. 1082–1093, Jun. 2019.

[6] R. A. Athamneh, D. B. Hani, H. Ali, and S. Hamasha, "Fatigue life degradation modeling of SnAgCu solder joints after aging," *IEEE Trans. Compon., Packag., Manuf. Technol.*, vol. 10, no. 7, pp. 1175–1184, Jul. 2020.

[7] H. Gopalakrishna *et al.*, "Activation energy for end-of-life solder bond degradation: Thermal cycling of field-aged PV modules," *IEEE J. Photovolt.*, vol. 10, no. 6, pp. 1762–1771, Nov. 2020.

[8] S. H. Ali, M. Heydarzadeh, S. Dusmez, X. Li, A. S. Kamath, and B. Akin, "Lifetime estimation of discrete IGBT devices based on Gaussian process," *IEEE Trans. Ind. Appl.*, vol. 54, no. 1, pp. 395–403, Jan. 2018.

[9] W. A. Siswanto, M. Arun, I. V. Krasnopevtseva, A. Surendar, and A. Maseleno, "A competition between stress triaxiality and Joule heating on microstructure evolution and degradation of SnAgCu solder joints," *J. Manuf. Processes*, vol. 54, pp. 221–227, Jun. 2020.

[10] X. Long, X. He, and Y. Yao, "An improved unified creep-plasticity model for SnAgCu solder under a wide range of strain rates," *J. Mater. Sci.*, vol. 52, no. 10, pp. 6120–6137, May 2017.

[11] X. Long, Z. Chen, W. Wang, Y. Fu, and Y. Wu, "Parameterized Anand constitutive model under a wide range of temperature and strain rate: Experimental and theoretical studies," *J. Mater. Sci.*, vol. 55, no. 24, pp. 10811–10823, Aug. 2020.

[12] Y. Jia, Y. Huang, F. Xiao, H. Deng, Y. Duan, and F. Iannuzzo, "Impact of solder degradation on VCE of IGBT module: Experiments and modeling," *IEEE J. Emerg. Sel. Topics Power Electron.*, early access, Jul. 12, 2019, doi: 10.1109/JESTPE.2019.2928478.

[13] S.-P. Zhu, H.-Z. Huang, L.-P. He, Y. Liu, and Z. Wang, "A generalized energy-based fatigue-creep damage parameter for life prediction of turbine disk alloys," *Eng. Fract. Mech.*, vol. 90, pp. 89–100, Jan. 2012.

[14] R. Bayerer, T. Herrmann, T. Licht, J. Lutz, and M. Feller, "Model for power cycling lifetime of IGBT modules–various factors influencing lifetime," in *Proc. 5th Int. Conf. Integr. Power Electron. Syst.*, 2008, pp. 1–6.

[15] B. Gao *et al.*, "A temperature gradient-based potential defects identification method for IGBT module," *IEEE Trans. Power Electron.*, vol. 32, no. 3, pp. 2227–2242, Mar. 2017.

[16] S. Baba, A. Gieraltowski, M. Jasinski, F. Blaabjerg, A. S. Bahman, and M. Zelechowski, "Active power cycling test bench for SiC power MOSFETs—Principles, design, and implementation," *IEEE Trans. Power Electron.*, vol. 36, no. 3, pp. 2661–2675, Mar. 2021.

[17] S. Zhao, S. Chen, F. Yang, E. Ugur, B. Akin, and H. Wang, "A composite failure precursor for condition monitoring and remaining useful life prediction of discrete power devices," *IEEE Trans. Ind. Informat.*, vol. 17 no. 1, pp. 688–698, Jan. 2021.

[18] U.-M. Choi, F. Blaabjerg, and S. Jørgensen, "Power cycling test methods for reliability assessment of power device modules in respect to temperature stress," *IEEE Trans. Power Electron.*, vol. 33, no. 3, pp. 2531–2551, Mar. 2018.

[19] D. Kim *et al.*, "On-line thermal resistance and reliability characteristic monitoring of power modules with Ag sinter joining and Pb, Pb-free solders during power cycling test by SiC TEG chip," *IEEE Trans. Power Electron.*, vol. 36, no. 5, pp. 4977–4990, May 2020.

[20] E. R, G. Kavithaa, V. Samavatian, K. Alhaifi, A. Kokabi, and H. Moayedi, "Reliability enhancement of a power semiconductor with optimized solder layer thickness," *IEEE Trans. Power Electron.*, vol. 35, no. 6, pp. 6397–6404, Jun. 2020.

[21] C.-H. Lee, K.-C. Wu, and K.-N. Chiang, "A novel acceleration-factor equation for packaging-solder joint reliability assessment at different thermal cyclic loading rates," *J. Mech.*, vol. 33, no. 1, pp. 35–40, 2017.

[22] W. Wang, Z. Chen, S. Wang, and X. Long, "Mechanics-based acceleration for estimating thermal fatigue life of electronic packaging structure," *Microelectron. Rel.*, vol. 107, Apr. 2020, Art. no. 113616.

[23] G. Ren, M. N. Collins, J. Punch, E. Dalton, and R. Coyle, *Pb-Free Solder-Microstructural, Material Reliability, and Failure Relationships*, A. S. H. Makhlouf M. Aliofkhazraei, Eds. Oxford, U.K.: Butterworth-Heinemann, 2020, pp. 107–151.

[24] S. Hamasha, A. Qasaimeh, Y. Jaradat, and P. Borgesen, "Correlation between solder joint fatigue life and accumulated work in isothermal cycling," *IEEE Trans. Compon., Packag., Manuf. Technol.*, vol. 5, no. 9, pp. 1292–1299, Sep. 2015.

[25] R. Al Athamneh and S. Hamasha, "Fatigue behavior of SAC-bi and SAC305 solder joints with aging," *IEEE Trans. Compon., Packag., Manuf. Technol.*, vol. 10, no. 4, pp. 611–620, Apr. 2020.

[26] E. Dalton, G. Ren, J. Punch, and M. N. Collins, "Accelerated temperature cycling induced strain and failure behaviour for BGA assemblies of third generation high ag content Pb-free solder alloys," *Mater. Des.*, vol. 154, pp. 184–191, Sep. 2018.

[27] R. Berni, M. Catelani, C. Fiesoli, and V. L. Scarano, "A comparison of alloy-surface finish combinations considering different component package types and their impact on soldering reliability," *IEEE Trans. Rel.*, vol. 65, no. 1, pp. 272–281, Mar. 2016.

[28] H. Ma, M. Ahmad, and K.-C. Liu, "Reliability of lead-free solder joints under a wide range of thermal cycling conditions," *IEEE Trans. Compon., Packag., Manuf. Technol.*, vol. 1, no. 12, pp. 1965–1974, Dec. 2011.

[29] H. Behjati and A. Davoudi, "Reliability analysis framework for structural redundancy in power semiconductors," *IEEE Trans. Ind. Electron.*, vol. 60, no. 10, pp. 4376–4386, Oct. 2013.

[30] H. Behjati and A. Davoudi, "Comparative reliability study of hybrid energy storage systems in hybrid electric vehicles," in *Proc. IEEE Transp. Electrific. Conf. Expo. (ITEC)*, Jun. 2012, pp. 1–6.

[31] H. Behjati and A. Davoudi, "Reliability analysis framework for structural redundancy in power semiconductors," *IEEE Trans. Ind. Electron.*, vol. 60, no. 10, pp. 4376–4386, Oct. 2013.

[32] *MIL-HDBK-217F*, Reliab. Predict. Electron. Equipment, U.S. Dep. Def., 1995.

[33] *IEEE Guide for Selecting and Using Reliability Predictions Based on IEEE 1413*, Standard 1413.1-2002, 2003.

[34] I.-R. Chen and F. B. Bastani, "Effect of artificial-intelligence planning-procedures on system reliability," *IEEE Trans. Rel.*, vol. 40, no. 3, pp. 364–369, Aug. 1991.
[35] T. Dragičević, P. Wheeler, and F. Blaabjerg, "Artificial intelligence aided automated design for reliability of power electronic systems," *IEEE Trans. Power Electron.*, vol. 34, no. 8, pp. 7161–7171, Aug. 2019.
[36] V. Samavatian, M. Fotuhi-Firuzabad, M. Samavatian, P. Dehghanian, and F. Blaabjerg, "Correlation-driven machine learning for accelerated reliability assessment of solder joints in electronics," *Sci. Rep.*, vol. 10, no. 1, Dec. 2020, Art. no. 14821.
[37] I. Labed and D. Labed, "Extreme learning machine-based alleviation for overloaded power system," *IET Gener., Transmiss. Distrib.*, vol. 13, no. 22, pp. 5058–5070, Nov. 2019.
[38] J. L. Cremer, I. Konstantelos, and G. Strbac, "From optimization-based machine learning to interpretable security rules for operation," *IEEE Trans. Power Syst.*, vol. 34, no. 5, pp. 3826–3836, Sep. 2019.
[39] B. Pozo, J. Garate, S. Ferreiro, I. Fernandez, and E. Fernandez de Gorostiza, "Supercapacitor electro-mathematical and machine learning modelling for low power applications," *Electronics*, vol. 7, no. 4, p. 44, Mar. 2018.
[40] D. Zhang, X. Han, and C. Deng, "Review on the research and practice of deep learning and reinforcement learning in smart grids," *CSEE J. Power Energy Syst.*, vol. 4, no. 3, pp. 362–370, Sep. 2018.
[41] S. Yi and R. Jones, "Machine learning framework for predicting reliability of solder joints," *Soldering Surf. Mount Technol.*, vol. 32, no. 2, pp. 82–92, Aug. 2019.
[42] V. Samavatian, H. Iman-Eini, Y. Avenas, and M. Samavatian, "Effects of creep failure mechanisms on thermomechanical reliability of solder joints in power semiconductors," *IEEE Trans. Power Electron.*, vol. 35, no. 9, pp. 8956–8964, Sep. 2020.
[43] A. Surendar, V. Samavatian, A. Maseleno, A. Z. Ibatova, and M. Samavatian, "Effect of solder layer thickness on thermo-mechanical reliability of a power electronic system," *J. Mater. Sci. Mater. Electron.*, vol. 29, no. 17, pp. 15249–15258, Sep. 2018.
[44] J. Xiong, S.-Q. Shi, and T.-Y. Zhang, "A machine-learning approach to predicting and understanding the properties of amorphous metallic alloys," *Mater. Des.*, vol. 187, Feb. 2020, Art. no. 108378.
[45] Z. Tang and P. A. Fishwick, "Feedforward neural nets as models for time series forecasting," *ORSA J. Comput.*, vol. 5, no. 4, pp. 374–385, Nov. 1993.
[46] S. Sun, R. Ouyang, B. Zhang, and T.-Y. Zhang, "Data-driven discovery of formulas by symbolic regression," *MRS Bull.*, vol. 44, no. 7, pp. 559–564, Jul. 2019.
[47] V. Samavatian, H. Iman-Eini, Y. Avenas, and S. Shemehsavar, "Reciprocal and self-aging effects of power components on reliability of DC–DC boost converter with coupled and decoupled thermal structures," *IEEE Trans. Compon., Packag., Manuf. Technol.*, vol. 9, no. 12, pp. 2506–2513, Dec. 2019.
[48] V. Samavatian, Y. Avenas, and H. Iman-Eini, "Mutual and self-aging effects of power semiconductors on the thermal behaviour of DC-DC boost power converter," *Microelectron. Rel.*, vols. 88–90, pp. 493–499, Sep. 2018.
[49] V. Samavatian, H. Imaneini, and Y. Avenas, "Reliability assessment of multistate degraded systems: An application to power electronic systems," *IEEE Trans. Power Electron.*, vol. 35, no. 4, pp. 4024–4032, Apr. 2019.
[50] M. Eftekhari and A. Fatemi, "Creep-fatigue interaction and thermo-mechanical fatigue behaviors of thermoplastics and their composites," *Int. J. Fatigue*, vol. 91, pp. 136–148, Oct. 2016.
[51] D. W. A. Rees, "Life prediction techniques for combined creep and fatigue," *Prog. Nucl. Energy*, vol. 19, no. 3, pp. 211–239, Jan. 1987.
[52] P. Hegde, D. C. Whalley, and V. V. Silberschmidt, "Creep damage study at powercycling of lead-free surface mount device," *Comput. Mater. Sci.*, vol. 45, no. 3, pp. 638–645, May 2009.
[53] D. K. Joo, J. Yu, and S. W. Shin, "Creep rupture of lead-free Sn-3.5Ag-Cu solders," *J. Electron. Mater.*, vol. 32, no. 6, pp. 541–547, Jun. 2003.
[54] Y. Chen, Y. Jin, and R. Kang, "Coupling damage and reliability modeling for creep and fatigue of solder joint," *Microelectron. Rel.*, vol. 75, pp. 233–238, Jan. 2017.
[55] X. Hu, T. Xu, L. M. Keer, Y. Li, and X. Jiang, "Shear strength and fracture behavior of reflowed $Sn_{3.0}Ag_{0.5}Cu$/Cu solder joints under various strain rates," *J. Alloys Compounds*, vol. 690, pp. 720–729, Jan. 2017.
[56] X. Chen, J. Zhou, F. Xue, and Y. Yao, "Mechanical deformation behavior and mechanism of sn-58Bi solder alloys under different temperatures and strain rates," *Mater. Sci. Eng., A*, vol. 662, pp. 251–257, Apr. 2016.
[57] W. J. Plumbridge and C. R. Gagg, "Effects of strain rate and temperature on the stress-strain response of solder alloys," *J. Mater. Sci. Mater. Electron.*, vol. 10, no. 5, pp. 461–468, 1999.
[58] Y. Chen, Y. Jin, and R. Kang, "Microelectronics reliability coupling damage and reliability modeling for creep and fatigue of solder joint," *Microelectron. Reliab.*, vol. 75, pp. 233–238, Dec. 2017.
[59] D. Ghaderi, M. Pourmahdavi, V. Samavatian, O. Mir, and M. Samavatian, "Combination of thermal cycling and vibration loading effects on the fatigue life of solder joints in a power module," *Proc. Inst. Mech. Eng. L, J. Mater., Design Appl.*, vol. 233, no. 9, pp. 1753–1763, Jun. 2018.